

Collective Josephson vortex dynamics in a finite number of intrinsic Josephson junctions

Myung-Ho Bae¹, Jae-Hyun Choi¹, and Hu-Jong Lee^{1,2,*}

¹Department of Physics, Pohang University of Science and Technology, Pohang 790-784, Republic of Korea and

²National Center for Nanomaterials Technology, Pohang 790-784, Republic of Korea

(Dated: May 13, 2010)

We report the experimental confirmation of the collective transverse plasma modes excited by the Josephson vortex lattice in stacks of intrinsic Josephson junctions in $\text{Bi}_2\text{Sr}_2\text{CaCu}_2\text{O}_{8+x}$ single crystals. The excitation was confirmed by analyzing the temperature (T) and magnetic field (H) dependencies of the multiple sub-branches in the Josephson-vortex-flow region of the current-voltage characteristics of the system. In the near-static Josephson vortex state for a low tunneling bias current, pronounced magnetoresistance oscillations were observed, which represented a triangular-lattice vortex configuration along the c axis. In the dynamic vortex state in a sufficiently high magnetic field and for a high bias current, splitting of a single Josephson vortex-flow branch into multiple sub-branches was observed. Detailed examination of the sub-branches for varying H field reveals that sub-branches represent the different modes of the Josephson-vortex lattice along the c axis, with varied configuration from a triangular to a rectangular lattices. These multiple sub-branches merge to a single curve at a characteristic temperature, above which no dynamical structural transitions of the Josephson vortex lattice is expected.

PACS numbers: 74.72.Hs, 74.50.+r, 74.78.Fk, 85.25.Cp

I. INTRODUCTION

It has been known that stacked intrinsic Josephson junctions (IJJs) form in naturally grown $\text{Bi}_2\text{Sr}_2\text{CaCu}_2\text{O}_{8+x}$ (Bi-2212) single crystals.¹ The collective Josephson plasma oscillation, manifested by the electromagnetic resonant absorption in such Josephson-coupled layered superconductors, has provided the key to understanding the superconducting state and the vortex phases² forming in the materials. Two kinds of collective Josephson plasma modes, *longitudinal* and *transverse*, exist in such a system of an *infinite number* of stacked IJJs.³ The longitudinal plasma mode oscillation, excited in an externally applied c -axis-oscillating electric field, propagates along the c axis of a stack of IJJs with the inter-layer phase difference of a junction being uniform in a planar direction. The resonant absorption of externally applied microwaves by the excitation of the longitudinal modes enables one to directly obtain the Josephson plasma frequency, ω_p . This, in turn, provides information on the interlayer Josephson coupling strength and the c -axis superfluid density in Bi-2212.⁴ By contrast, the transverse plasma modes can be excited by the oscillating magnetic fields in the ab plane. The resulting induced current along the c axis generates the oscillating electric field that resonates with the transverse Josephson plasma oscillation.

On the other hand, a system with a *finite number* (N) of stacked IJJs, described by linearized coupled sine-Gordon differential equations with the inductive interjunction coupling, exhibits *collective transverse plasma* (CTP) eigen modes, with the eigen frequencies lying between those of the longitudinal and the transverse modes found for a system of an infinite number of stacked junctions.^{5,6} The corresponding dispersion relation is ex-

pressed as

$$\omega_n(k) = \omega_p \sqrt{1 + \frac{\lambda_c^2 k^2}{1 + (2\lambda_{ab}^2/sD)(1 - \cos(\frac{\pi n}{N+1}))}}. \quad (1)$$

Here, λ_{ab} (λ_c) is the c -axis (ab -plane) London penetration depth, N the number of the junctions in a stack, $s=0.3$ nm ($D=1.2$ nm) the thickness of a superconducting (insulating) layer, $k(=2\pi m/L$; L =the length of a stack; m =the number of the vortices present in a junction) the wave number of the plasma oscillation.⁵ The mode index n runs from 1 to N .

The CTP modes can be excited by the moving Josephson vortex lattice forming in high magnetic fields, which are alternative solutions of the coupled sine-Gordon equations.⁷ The temporal oscillation of the inter-layer phase difference due to the moving Josephson vortex lattice, with the frequency matching with that of any CTP modes, excites a resonant plasma oscillation. The Josephson vortex lattice also transforms its spatial configuration along the c axis in accordance with the c -axis standing-wave modes of the plasma oscillation. The resonance of Josephson vortex lattice to the CTP modes is revealed in the form of the multiple Josephson vortex-flow branches in the tunneling current-voltage (I - V) characteristics of a stack of IJJs.^{8,9}

Experimental observation of the multiple CTP modes in a stack of a finite number of IJJs has often been attempted in a mesa or an S-shaped stack of IJJs fabricated on the surface of a large stack of IJJs, which is called a pedestal or a basal layer.^{10,11} Since each superconducting bilayer in a stack of IJJs is much thinner than the c -axis London penetration depth λ_{ab} , Josephson vortices in a usual mesa or an S-shaped-stack structure are in a strong inductive coupling to those in the basal layer that

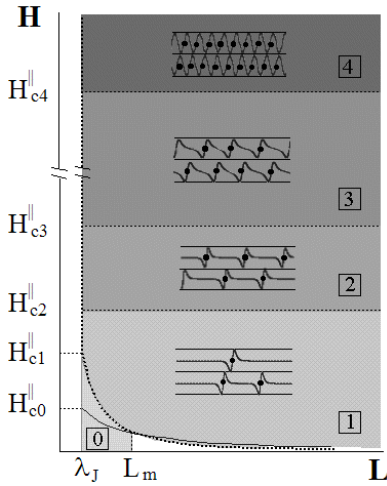


FIG. 1: The phase diagram of the Josephson vortex configuration for different ranges of transverse magnetic field and the length of the intrinsic-Josephson-junction stack. A schematic figure in the each region represents the supercurrent distributions in layered structures, where the centers of the Josephson vortices are indicated by black dots.

contains a large number of IJJs by itself, although measurements are intended to be made on a finite number of stacks in the structure of interest. Thus, the stack of IJJs with a coupling to the basal layers corresponds to a system containing nearly an infinite number of junctions, which does not support the CTP mode formation along the c axis. This situation significantly affects the dynamics of the Josephson vortices in the mesa or the S-shaped stack itself. This may explain the usual failure of observing the multiple resonating modes in those structures.

In this paper, we present the static and dynamic states of Josephson vortices in stacks of IJJs, each sandwiched between two Au electrodes without the basal layer, thus consisting of a genuinely finite number of IJJs. In the near-static state in a low tunneling bias current on a single Josephson vortex-flow branch, pronounced magnetoresistance oscillations were observed with $h/4e$ magnetic flux period. This half-flux-quantum periodic resistance oscillations indicate that the Josephson vortex lattice in the near-static state constitutes a triangular lattice along the c axis. In the dynamic state in a high tunneling bias current, on the other hand, a single Josephson vortex-flow branch splits into multiple sub-branches. Detailed examination of the sub-branches for varying magnetic fields and temperatures revealed that the observed sub-branches were caused by the resonance between the Josephson vortex lattices and the CTP modes.

II. BASIC CONCEPTS

The Josephson vortex configuration in stacked IJJs of Bi-2212 single crystals is determined by the magnetic flux density in the junctions and the junction size.¹² Josephson vortices are introduced to the insulating layer of a junction when its length L is longer than the Josephson penetration depth, $\lambda_J [= \sqrt{\Phi_0/2\pi\mu_0 j_c(D + 2\lambda_{ab}^2/s)}]$, where $\Phi_0 (= h/2e)$ is a flux quantum. One can identify various characteristic magnetic fields in relation with the dynamics of Josephson vortices [see Fig. 1]. For a stack of junctions of length L Josephson vortices start entering the junctions above a characteristic field,^{13,14} $H_{c1}^{\parallel} [= (\Phi_0 \lambda_c / L^2 \lambda_{ab}) \ln(\lambda_{ab}/D)]$. This field can be higher than the nominal value of one flux quantum threading a junction of length L , that is $H_{c0}^{\parallel} (= \Phi_0 / (s + D)L)$, especially for a junction comparable to λ_J . Even above H_{c0}^{\parallel} the tunneling screening current prevents an external magnetic field from entering the junctions until it reaches H_{c1}^{\parallel} . Thus, for a junction with its length in the range of $\lambda_J < L < L_m [= \lambda_J \ln(\lambda_{ab}/(s + D))]$, one can observe the usual oscillatory Fraunhofer modulation of the tunneling critical current as a function of an external magnetic field of $H < H_{c1}^{\parallel}$, although the junction size is larger than λ_J (Region 0).¹⁵

The Josephson vortices entering the junctions for $H > H_{c1}^{\parallel}$ form a regular lattice as the magnetic field reaches the value¹⁶ $H_{c2}^{\parallel} (= 1.4\Phi_0/2\pi(s+D)\lambda_J)$. In this field range (Region 1), since the field-induced vortices exist in arbitrary configurations in a given magnetic field, disordered multiple vortex-flow subbranches are generated in the I - V characteristics. In this region, the number of vortices in a junction and the propagation velocities of different vortex configurations are not correlated with each other.¹⁷ Thus, in this field range, the vortex-flow subbranches in the I - V characteristics are not related to vortex mode velocities^{6,18} or geometrical resonances.¹⁹

In an external field above H_{c2}^{\parallel} (Region 2), Josephson vortices start forming a triangular lattice. Recent observation of the oscillatory vortex-flow resistance arising from the interaction between the vortex lattice and the crystal boundary potential clearly confirmed the existence of the triangular vortex lattice^{20,21} above H_{c2}^{\parallel} .

On the other hand, the resonance between the Josephson vortex lattice and CTP modes is well known in this vortex dynamics system.⁶ The collective resonance revealed as voltage peaks (in the case of the voltage bias) or voltage jumps (in the case of the current bias) has been searched extensively both theoretically and experimentally.^{5,10,22} The collective resonance has been observed in the dense-vortex state corresponding to the field range of $H > H_{c3}^{\parallel} [= \Phi_0/2\lambda_J(s + D)]$, where the shortest inter-vortex spacing becomes comparable to the diameter of a Josephson vortex $2\lambda_J$ (Region 3). Thus, Josephson vortices in Regions 2 and 3, although they form triangular lattices in both regions in a static state

without a tunneling bias current (Fig. 1), behave differently in the vortex-flow state in the presence of a finite tunneling bias current. In the dynamic state, Josephson vortices in Region 2 remains in a triangular lattice, while those in Region 3 transform their lattice configuration to fit the plasma propagation modes in the stacked junctions.²³ The non-Josephson-like emission from the Josephson-vortex motion²⁴ and the Shapiro resonance steps in the Josephson vortex-flow state²⁵ have been observed in this dense-vortex state. These results confirm the existence of the coherent motion of the Josephson vortex lattice through the entire thickness of stacked (intrinsic) Josephson junctions.

For the highest characteristic field H_{c4}^{\parallel} [$=\Phi_0/\lambda_J(s+D)$ (~ 4 T for Bi-2212)], the shortest inter-vortex spacing becomes comparable to the Josephson penetration depth,²⁶ λ_J . In this region (Region 4), the Josephson current along the length of a junction distributes almost sinusoidally so that the collective resonance behavior between the vortex motion and the plasma modes is expected to be stronger than in a field lower than H_{c4}^{\parallel} .

III. EXPERIMENT

As-grown slightly overdoped Bi-2212 single crystals were prepared by the conventional self-flux method. We fabricated, using the double-side cleaving technique,²⁷ three samples of IJJs sandwiched between two Au electrodes at the top and the bottom of a stack of IJJs without the basal part [Fig. 2(b)]. This structure, which is in contrast to the usual mesa or the S-shaped-stack structure fabricated on the surface of a single crystal with a large basal layer, is more coincident with the model systems usually adopted in the theoretical analysis.¹⁸ The geometry with the basal layer eliminated by the double-side cleaving enables one to investigate the Josephson vortex dynamics in coupled IJJs without the interference from the vortex motion in the basal layer. Furthermore, the top and the bottom Au-film leads in a stack help

the formation of the standing plasma oscillation modes along the c axis, while forming a transmission guide of the plasma oscillations along the length of the stack.

The samples containing sandwiched stacks were prepared in the following way.²⁸ A single crystal was first glued on a sapphire substrate using negative photoresist and was cleaved until an optically clean and flat surface was obtained. Then, a 100-nm-thick Au film was thermally deposited on top of the crystal to protect the surface of the crystal and to make a good ohmic contact. A mesa structure was then prepared by photolithographic patterning and Ar-ion-beam etching. The surface of the patterned mesa was fixed to another sapphire substrate using negative photoresist and the basal layer of the mesa was subsequently cleaved away. This process, called the double-side-cleaving technique, was developed by Wang *et al.*²⁷ A 100-nm-thick Au film was again deposited on this freshly cleaved crystal surface, leaving a stack of IJJs sandwiched between two Au electrodes. A few- μm -long portions on both sides of the sandwiched stack were etched away subsequently [see Fig. 2(a)] to get the bottom Au electrode exposed for c -axis transport measurements as schematically depicted in Fig. 2(b). Finally, a 300-nm-thick Au-extension pad was attached on each of the Au electrode. The lateral sizes of three samples were $13.5 \times 1.4 \mu\text{m}^2$ [SP1], $15 \times 1.4 \mu\text{m}^2$ [SP2] and $16 \times 1.5 \mu\text{m}^2$ [SP3].

The magnetic field was aligned in parallel with the plane of junctions within the resolution of 0.01 degree to minimize the pinning of Josephson vortices by the pancake vortices that can form in CuO_2 bilayers due to the vertical component of a misaligned field. The alignment was done, in a field of 4 T and at a temperature around 60 K, by tuning to the angle that gives the maximum Josephson-vortex-flow resistance or the minimum pinning of the Josephson vortices by the pancake vortices generated by the angle misalignment.¹⁰ To minimize the external noise, transport measurements were performed with a low-pass filter connected to each electrode located at room temperature.

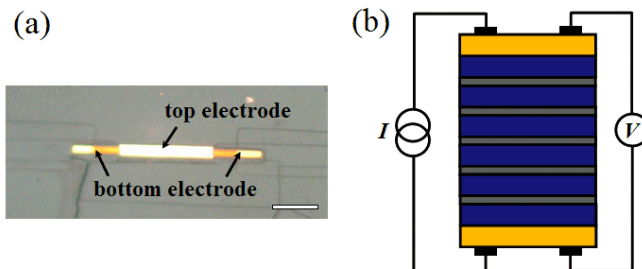


FIG. 2: (color online) (a) An optical micrograph of a sample during the fabrication process. The scale bar represents the length of $10 \mu\text{m}$. (b) Schematics of sample and measurement configurations.

TABLE I: Sample parameters. N is the total number of intrinsic Josephson junctions in a stack, λ_J the Josephson penetration depth, $H_{c3}^{\parallel}=\Phi_0/2\lambda_J(s+D)$ (s and D the thickness of the superconducting and the insulating layers, respectively), c_m the maximum propagation velocity of vortices in Region 3, and c_1 the velocity of the fastest collective plasma mode estimated by the RCSJ model.

sample number	stack size (μm^2)	N	λ_J (μm)	H_{c3}^{\parallel} (T)	c_m ($\times 10^5 \text{ m/s}$)	c_1 ($\times 10^5 \text{ m/s}$)
SP1	13.5×1.4	35	0.25	2.8	3.8	3.5
SP2	15×1.4	22	0.32	2.1	3.9	3.7
SP3	16×1.5	45	0.24	2.9	4.2	3.5

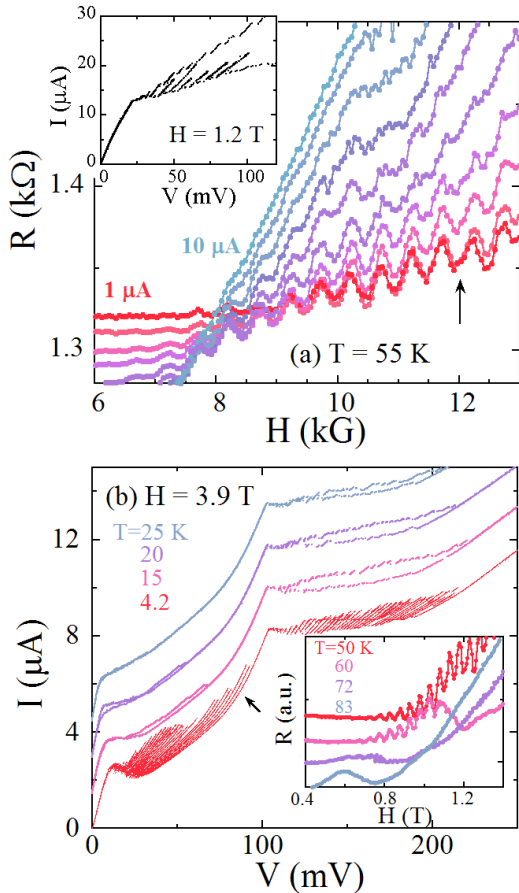


FIG. 3: (color online) (a) The Josephson vortex-flow resistance, R as a function of an external magnetic field H for SP1 at $T=55$ K in bias currents from $1\ \mu\text{A}$ to $10\ \mu\text{A}$ at intervals of $1\ \mu\text{A}$. (b) Temperature dependence of the Josephson-vortex-flow sub-branches and quasiparticle branches of SP1 at $H=3.9$ T. Inset of (a): a single Josephson vortex-flow branch and quasiparticle tunneling branches in $H=1.2$ T at $T=55$ K. Inset of (b): the temperature dependence of $R(H)$ in a bias current of $3\ \mu\text{A}$. Curves in the main panel and the inset of (b) are shifted vertically for clarity.

IV. RESULTS AND DISCUSSION

A. Static and dynamic state

Fig. 3(a) shows the oscillation of Josephson-vortex-flow resistance of SP1 [$N=35$] as a function of external magnetic fields at $T=55$ K in bias currents from $1\ \mu\text{A}$ to $10\ \mu\text{A}$ at intervals of $1\ \mu\text{A}$. The field period of the oscillation, $H_p=510\ \text{G}$ is one half of H_0 ($=\Phi_0/L(s+D)$) through the junction area of length $L=13.5\ \mu\text{m}$ and thickness ($s+D$)= $1.5\ \text{nm}$. The oscillation of the Josephson-vortex-flow resistance is known to be caused by the interaction between the triangular Josephson vortex lattice along the c axis and the vortex-flow boundary potential at the junction edges.^{20,21,29} The observation of the Josephson-vortex-flow resistance oscillation in our sand-

wiched stack without the basal layers indicates that, as the S-shaped-stack geometry, our sandwiched geometry also supports the Josephson-vortex triangular lattice in the steady state [see the inset of Fig. 4(a)]. The oscillation in Fig. 3(a) is reduced by increasing bias current as the bias current tilts the boundary potential.³⁰ The oscillatory-magnetoresistance behavior is also suppressed completely at $T \sim 80$ K near T_c ($=92$ K) as in the inset of Fig. 3(b), which is related to melting of the near-static Josephson vortex lattice.³¹

The inset of Fig. 3(a) shows the single Josephson-vortex-flow branch (the low-bias region) and quasiparticle branches (the high-bias region) in $H=1.2$ T at $T=55$ K. The field, belonging to Region 2 in Fig. 1, corresponds to the position indicated by the arrow in the main panel. In this field region, the single-curve Josephson-vortex-flow branch caused by the triangular lattice persists even down to 4.2 K (not shown). In Fig. 3(b), I - V characteristics in a field of Region 3 at $T=25$ K also show a single Josephson vortex-flow branch corresponding to the triangular lattice. Table I shows the characteristic field value of H_{c3}^{\parallel} of each sample.

Contrary to the field range of Region 2, however, the single Josephson-vortex-flow branch in Region 3 evolves into the multiple Josephson-vortex-flow sub-branches with decreasing temperature. Fig. 3(b) shows the temperature dependence of the Josephson-vortex-flow branches, where the multiple sub-branches start appearing at $T \sim 20$ K and become clearer with decreasing temperature. At $T=4.2$ K, a single branch representing the triangular lattice below the current bias of $I_b \sim 2\ \mu\text{A}$ splits into multiple Josephson-vortex-flow sub-branches for the higher current bias. The Josephson vortex flow, then, transits to the McCumber quasiparticle tunneling for I_b above $8\ \mu\text{A}$. The multiple Josephson-vortex-flow sub-branches rapidly suppress with increasing temperature above 4.2 K and disappear completely as the temperature reaches 25 K. On the contrary, the quasiparticle-tunneling branches are robust to the temperature variation and persist up to $T=25$ K. This contrasting temperature dependencies of two different regions strongly imply that the multiple branches in the two regions are of different physical origins.

We also observed the separation of the two characteristic multiple-branch regions in SP2 and SP3. Figs. 4(a) and 4(b) show the magnetic field dependencies of I - V characteristics of two sandwiched stacks, SP2 and SP3, respectively, at 4.2 K. The number of zero-field quasiparticle-tunneling branches of SP2 and SP3 were 22 and 45, respectively (not shown), which coincided with the total number of IJJs in the given stacks. The differentiation of the multiple branches by the collective Josephson vortex flow (the low-bias region) from the ones by the quasiparticle tunneling (the high-bias region) is based on the fact that the delimiting current, represented by the current values marked by the dotted vertical lines, stemmed from the zero-field Josephson critical current. Nonetheless, a finite resistance is present in the region

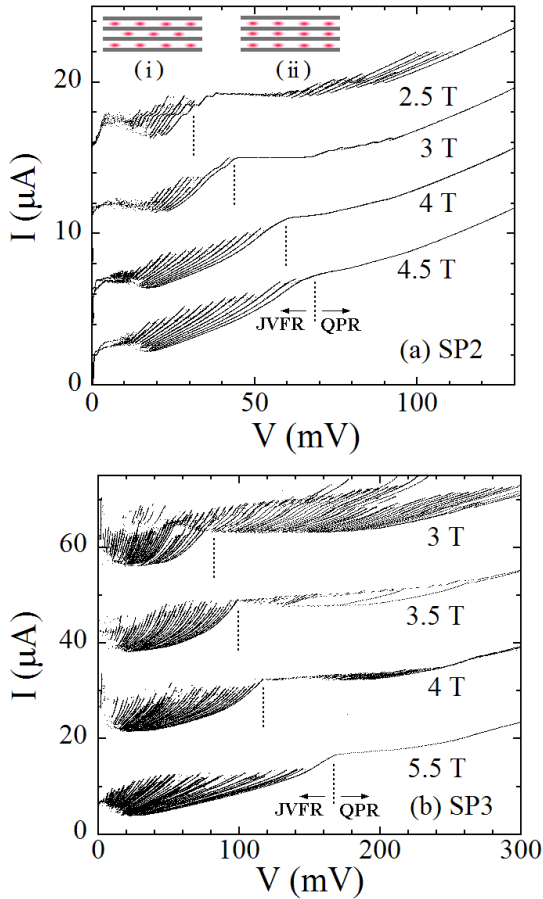


FIG. 4: (color online) The magnetic field dependencies of the Josephson vortex-flow sub-branches and the McCumber branches of (a) SP2 and (b) SP3 at $T=4.2$ K. The I - V characteristics in all the figures are shifted vertically for clarity. A voltage V_m denoted by a vertical dotted line in each set of curves demarcates the Josephson vortex flow region (JVFR) from the McCumber quasiparticle-tunneling region (QPR). Inset of (a): (i) the triangular lattice and (ii) the rectangular lattice configurations of the Josephson vortex lattice along the c axis. The contact resistance was subtracted numerically in the main panels of (a) and (b).

below the critical bias point because of the Josephson vortex flow, although the region itself represents the dissipationless pair tunneling state.

The observed sub-branches for SP2 and SP3 have common features: (i) a single Josephson-vortex-flow branch splits into multiple sub-branches for Regions 3 and 4, (ii) the number of the quasiparticle sub-branches is ~ 18 and ~ 42 , respectively, which is close to the number of the junctions in each sample, and (iii) the sub-branches in the Josephson vortex-flow region become clearer and wider with increasing the transverse magnetic field (in contrast to the case of quasiparticle sub-branches, which keep shrinking with field instead). These three common properties of sub-branches are consistent with the prediction of the inductive coupling theory for the electro-

dynamics of stacked Josephson junctions.

Since the speed of vortices, c_m , is limited by that of the maximum electromagnetic wave in a junction, Josephson-vortex-flow state changes to quasiparticle tunneling state near the maximum cut-off velocity or equivalently by the limiting voltage V_m in the outermost sub-branch. Using the relation⁹ of $V_m=NH(s+D)c_m$, we could get c_m as $\sim 3.9 \times 10^5$ m/s and $\sim 4.2 \times 10^5$ m/s for the corresponding delimiting bias point V_m in SP2 and SP3, respectively. These values are similar to those obtained from a Josephson-vortex-flow branch in mesa structures.¹⁰ In the case of the usual mesa or the S-shaped-stack structure with a basal layer, only a single Josephson-vortex-flow branch used to be observed below the critical bias point, regardless of the temperature and the magnetic field intensity. The velocity c_m corresponding to the delimiting value on this single branch has been regarded as the slowest mode velocity, $n=N$. As illustrated below, however, in our case without the basal layer c_m , corresponding to V_m in the outermost sub-branch, represents the propagation velocity of the $n=1$ plasma mode.

In the resistively and capacitively shunted junction (RCSJ) model³² the junction capacitance is obtained by the relation, $C_j=\beta_c \frac{\Phi_0}{2\pi I_c R_n^2}$, where β_c [$=(4I_c/\pi I_r)^2$] is the McCumber parameter, R_n is the normal-state junction resistance and I_r is the return current. In SP2, C_j is obtained to be about 47 pF, with $I_c(=0.2$ mA), $I_r(=4.8$ μ A) and $R_n(=10$ Ω). The Swihart velocity $c_0=\sqrt{sA/2\mu_0 C_j \lambda_{ab}^2}$, estimated from the junction capacitance, is 3.6×10^4 m/s, where $\lambda_{ab}=200$ nm and the junction area of $A=21$ μ m². The resulting fastest mode velocity $c_1=3.7 \times 10^5$ m/s is in remarkable agreement with the observed value of c_m in SP2. Experimental values of c_m in Table I are consistent with the calculated ones of c_1 for all three samples. This indicates that the outermost sub-branch is the fastest velocity, $n=1$, mode.

In general, Josephson-vortex resonance branches by the inter-layer inductive coupling have been predicted to generate current steps near the resonance voltages on the background of a single resistive branch.⁵ In the present study, however, Josephson-vortex resonance to the CTP modes constitutes multiple sub-branches over almost the entire bias range. A recent theory for an interlayer inductive coupling hybridized by a capacitive coupling predicts that the resistive sub-branches corresponding to the collective resonance modes show linear I - V characteristics in the low-bias region with the varied slopes from one another.³³ More spread in the slopes are predicted for a higher capacitive coupling. Fig. 5(a) shows the Josephson-vortex-flow sub-branches for SP2 at $H=5$ T. As predicted by the theory, all the sub-branches in the Josephson vortex-flow regime exhibit linearities with varied slopes in the low bias range. The extrapolation of the linear low-bias region converges to a single point on the current axis, although the inductive-capacitive hybrid coupling theory predicts they should converge to the origin. The discrepancy indicates a finite pinning of Josephson vortex motion due to the pre-

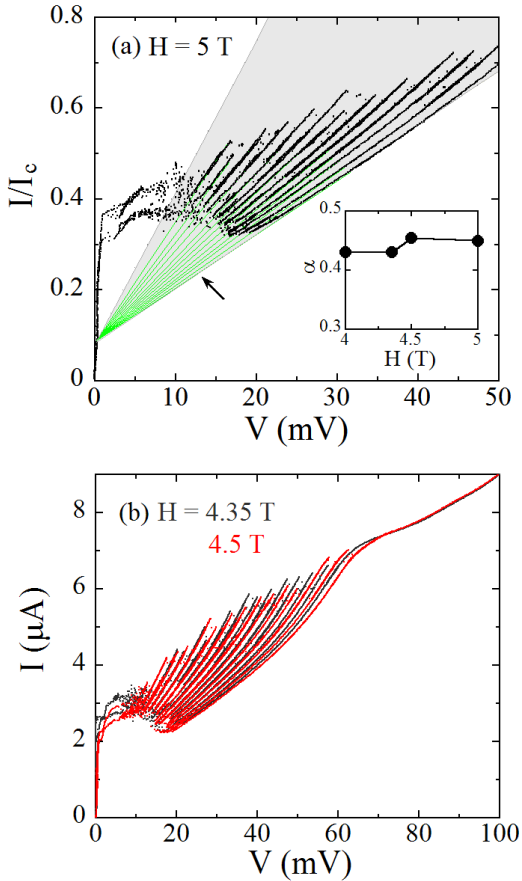


FIG. 5: (a) Josephson vortex-flow sub-branches for SP2 for $H=5$ T with the current axis normalized by the critical bias current. Splitting of the low-bias Josephson-vortex-flow curve into multiple sub-branches indicates the effectiveness of the inter-junction capacitive coupling. (b) Josephson vortex-flow sub-branches for SP2 at $H=4.35$ and 4.5 T. The contact resistance was subtracted numerically in (a) and (b). Inset of (a): magnetic field dependence of the capacitive coupling parameter, α .

ence of any defects in the stacked junctions or pancake vortices due to any field misalignment, with the converging current point corresponding to the depinning current. The inductive-capacitive hybrid coupling model indicates that the extent of the spread in the low-bias slope of the resonant branches is proportional to the strength of the capacitive coupling represented by the parameter α as $V_n = \left[\frac{I - I_p}{I_c} \right] \frac{V_c}{1 + 2\alpha[1 - \cos(n\pi/N)]}$, where $n=1,2,\dots,N$. Here, I_p is the depinning current of the Josephson-vortex, I_c is the tunneling critical Josephson current at a given applied field. Here V_c is the maximum mode voltage corresponding to a given bias current as represented by the curve denoted with an arrow in Fig. 5(a). The gray region illustrates the best fit to the sub-branches in the low-bias region. The best-fit value of α turns out to be 0.45 with $V_c=4.22$ mV. The best-fit values of α were found to be almost insensitive to magnetic fields as $\alpha=0.43\sim0.45$

for $H=4\sim5$ T [see the inset of Fig. 5(a)], which is consistent with the assumption of the capacitive coupling and reasonably close to the theoretical expectation³³ of $0.1 < \alpha < 0.4$. Therefore, as shown in the upper inset of Fig. 4(a), we consider that the first ($n=N$; the leftmost) and last ($n=1$; the rightmost) sub-branches correspond to (i) the triangular and (ii) the rectangular Josephson vortex lattices along the c axis, respectively.

Fig. 5(b) shows the change of Josephson-vortex-flow sub-branches for SP2 when magnetic field increases from $H=4.35$ T to 4.5 T. The more changes take place in the voltages between the two magnetic fields for branches in the higher voltages (branches more to the right). This behavior can be compared to the dispersion relation of Eq. (1), which states that the lower-index modes are more dispersive than the higher-index modes. Thus, the right-most branches among multiple Josephson-vortex sub-branches in Figs. 3–6 are again considered to represent the square vortex lattice [see the inset of Fig. 4(a)] corresponding to the $n=1$ plasma excitation mode.

The maximum number of vortex-flow sub-branches counted for various fields in SP2 is 20, which is two modes smaller than the number of quasiparticle branches (or, equivalently, than the number of junctions). Recently, Ryndyk³⁴ proposed that the additional dissipation due to the charge-imbalance relaxation due to quasiparticle injection in a junction can prevent the structural transformation of Josephson-vortex lattice along the c axis. In our sample geometry quasiparticles are injected directly from outside through the outermost two junctions, which may cause the non-equilibrium charge-imbalance effect in the two outermost CuO_2 bilayer. The resulting suppression of the configurational transformation of Josephson-vortex lattice reduces the number of observable resonance modes. For inner CuO_2 planes, on the other hand, with the pair tunneling for a bias below the critical current of the junction, the quasiparticle injection can be neglected.

B. Temperature dependence

Figs. 6(a) and (b) show the temperature dependences of I - V characteristics for SP2 in $H=5.2$ T and for SP3 in $H=3$ T, respectively. The temperature dependences of the sub-branches in the Josephson vortex-flow region and quasiparticle-tunneling region are much different from each other. Although not clearly illustrated in the figures the quasiparticle branches survived up to temperatures close to T_c . The sub-branches in the Josephson vortex-flow region, however, disappeared at a characteristic temperature T_{ch} , near 18 K and 28 K for SP2 and SP3, respectively, leaving a single branch as SP1 in Fig. 3(b). These characteristic temperatures are almost insensitive to the fields applied [see insets of Figs. 6(a) and (b)].

In the vortex flow state for the magnetic-field range of Regions 3 and 4 the triangular vortex configuration and the multiple-mode configuration resonating with the col-

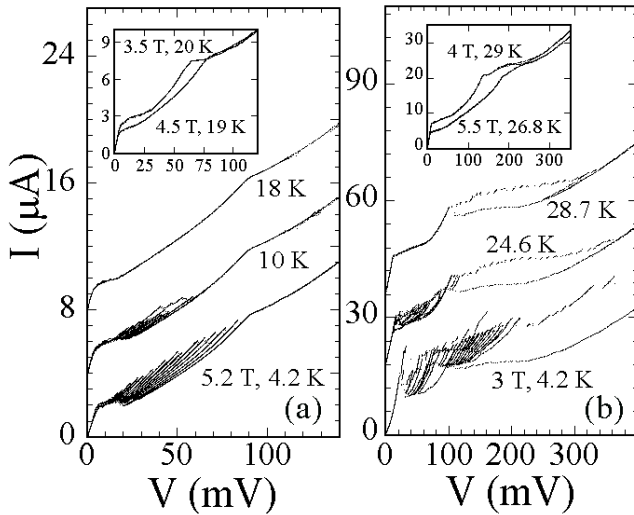


FIG. 6: Temperature dependence of I - V characteristics for (a) SP2 in $H=5.2$ T and (b) for SP3 in $H=3$ T. The curves are shifted vertically for clarity. The insets of (a) and (b) show a single Josephson vortex-flow branch above the characteristic temperature T_{ch} in two different magnetic fields for SP2 and SP3, respectively.

lective CTP modes compete each other. At low-enough temperatures, the triangular vortex configuration wins in the low-bias region, while the multiple-mode configuration predominates in the high-bias region. For $T \sim T_{ch}$, however, thermal fluctuation and quasiparticle dissipations prevent the Josephson vortex lattice from resonating with the collective CTP modes. Then the vortices stay on the triangular-lattice configuration without a structural transformation even in the dynamic state.³⁴ The value of V_m seems to be insensitive to temperature near T_{ch} , which means that the triangular Josephson vortex lattice can reach the maximum velocity corresponding to the fastest mode, $n=1$, without the structural transformation in resonance with the CTP modes. In this branch above T_{ch} , therefore, the lattice structure may be the modulated triangular lattice but with the propagation velocity still locked to that of the fastest mode. *Thus, the single branch above T_{ch} represents the triangular vortex lattice, while the well-defined outermost sub-branch below T_{ch} represents the rectangular lattice.* Accordingly, in Figs. 3(b) and 6, although the rightmost sub-branch below T_{ch} appears to directly transform into the single branch above T_{ch} , their characteristics correspond to very different Josephson-vortex configurations.

As mentioned earlier, the single Josephson vortex-flow branch without sub-branches has been observed in the usual mesa structure.¹⁰ In the usual mesa or the S-shaped-stack structure the structural transformation from the triangular lattice to the rectangular lattice in resonance to the CTP modes is hard to take place because of the strong coupling to the near-static triangular lattice in the basal layer even at sufficiently low temper-

atures. In this case, the velocity of the Josephson vortex lattice may reach that of the fastest mode without the structural transformation.³⁴

V. CONCLUSIONS

The Josephson vortex dynamics was comprehensively studied in compactly stacked intrinsic Josephson junctions over a wide range of magnetic fields and temperatures. Measurements were made on three stacks of intrinsic Josephson junctions, each sandwiched between two (top and bottom) normal-metallic electrodes, thus eliminating the interference from the basal layer(s). The I - V characteristics for high external magnetic fields (Regions 3 and 4 defined in Fig. 1) showed three states: (i) the near-static triangular Josephson-vortex state with the formation of a single branch, (ii) the dynamic vortex state with multiple-mode sub-branches, and (iii) the McCumber quasiparticle-tunneling state with quasiparticle sub-branches. In the dynamic vortex state, each sub-branch corresponded to the different configuration of the Josephson-vortex lattice along the c axis from a triangular to a rectangular lattices.⁵ With increasing temperature, the sub-branches disappeared at T_{ch} , above which no configurational transformation of the Josephson-vortex lattice can be assumed.

Due to the strong inductive coupling to many junctions in the basal layer(s), the mesa or the S-shaped-stack structure, although containing a finite number of junctions in the stack under study, behaves effectively as consisting of an infinite number of junctions along the c axis. Thus, these structures cannot support the formation of the multiple Josephson-vortex-flow modes as predicted theoretically for a finite number of junctions. Although the c -axis boundary condition is not strictly imposed in these systems the transverse vortex motion is still restricted by the boundary conditions at the side edges. This is the main reason why, in the mesa or the S-shaped-stack structure, clear magnetoresistance oscillations are observed by the interplay between the near-static triangular Josephson-vortex configuration²¹ and the boundary potential in the systems, while the transverse Josephson-vortex multiple modes are not obtained. One should be noted that the multiple collective Josephson vortex modes can be obtained only in a stack containing a finite number of (intrinsic) Josephson junctions. The triumph of this study is that our samples truly satisfied this condition of a finite number of junctions in a stack and, as a result, both the near-static Josephson vortex state highly coupled to the edge potential and the collective transverse Josephson-vortex state were identified in each junction. This facilitated the detailed identification of the vortex configurations illustrated in Fig. 1.

ACKNOWLEDGMENTS

The authors wish to acknowledge stimulating discussions with R. Kleiner, H. B. Wang, S. M. Kim, M. Machida, Ju H. Kim, and S. Sakai. This work was supported by the National Research Laboratory pro-

gram administrated by Korea Science and Engineering Foundation (KOSEF). This paper was also supported by POSTECH Core Research Program.

*Electronic address: hjlee@postech.ac.kr

¹ R. Kleiner, F. Steinmeyer, G. Kunkel, and P. Müller, Phys. Rev. Lett. **68**, 2394 (1992).

² O. K. C. Tsui, N. P. Ong, Y. Matsuda, Y. F. Yan, and J. B. Peterson, Phys. Rev. Lett. **73**, 724 (1994); L. N. Bulaevskii, M. P. Maley and M. Tachiki, Phys. Rev. Lett. **74**, 801 (1995). Y. Matsuda, M. B. Gaifullin, K. Kumagai, K. Kadowaki, and T. Mochiku, Phys. Rev. Lett. **75**, 4512 (1995).

³ M. Tachiki, T. Koyama and S. Takahashi, Phys. Rev. B **50**, 7065 (1994); I. Kakeya, K. Kindo, K. Kadowaki, S. Takahashi, and T. Mochiku, Phys. Rev. B **57**, 3108 (1998).

⁴ M. B. Gaifullin, Y. Matsuda, N. Chikumoto, J. Shimoyama, K. Kishio, and R. Yoshizaki, Phys. Rev. Lett. **83**, 3928 (1999).

⁵ R. Kleiner, Phys. Rev. B. **50**, 6919 (1994);

⁶ M. Machida, T. Koyama, A. Tanaka, and M. Tachiki, Physica C **330**, 85 (2000).

⁷ M. Machida and M. Tachiki, Curr. Appl. Phys. **1**, 341 (2001).

⁸ J. U. Lee, P. Guptasarma, D. Hornbaker, A. El-Kortas, D. Hinks, and K. E. Gray, Appl. Phys. Lett. **71**, 1412 (1997); Y.-J. Doh, J. Kim, H. S. Chang, S. Chang, H.-J. Lee, K. T. Kim, W. Lee, and J. H. Choy, Phys. Rev. B **63**, 144523 (2001).

⁹ M.-H. Bae and H.-J. Lee, Phys. Rev. B **70**, 052506 (2004).

¹⁰ G. Hechtfischer, R. Kleiner, K. Schlenga, W. Walkenhorst, P. Müller, and H. L. Johnson, Phys. Rev. B **55**, 14638 (1997).

¹¹ K. Hirata, S. Ooi, and T. Mochiku, Physica C **362**, 114 (2001).

¹² A. E. Koshelev, Phys. Rev. B **66**, 224514 (2002).

¹³ J. R. Clem, M. W. Coffey, and Z. Hao, Phys. Rev. B **44**, 2732 (1991).

¹⁴ M. V. Fistul and G.F. Giuliani, Physica C **230**, 9 (1994).

¹⁵ Yu. I. Latyshev, J. E. Nevelskaya, and P. Monceau, Phys. Rev. Lett. **77**, 932 (1996).

¹⁶ R. Ikeda, J. Phys. Soc. Jpn. **71**, 587 (2002).

¹⁷ V. M. Krasnov, V. A. Oboznov, V. V. Ryazanov, N. Mros, A. Yurgens, and D. Winkler, Phys. Rev. B **61**, 766 (2000).

¹⁸ S. Sakai, P. Bodin, and N. F. Pedersen, J. Appl. Phys **73**, 2411 (1993).

¹⁹ V. M. Krasnov, N. Mros, A. Yurgens, and D. Winkler, Phys. Rev. B **59**, 8463 (1999).

²⁰ S. Ooi, T. Mochiku, and K. Hirata, Phys. Rev. Lett. **89**, 247002 (2002).

²¹ For a sufficiently short stack of junctions the boundary-potential effect induces a rectangular vortex lattice configuration in a steady state. For details, refer to M. Machida, Phys. Rev. Lett. **96**, 097002 (2006).

²² A. E. Koshelev and I. S. Aranson, Phys. Rev. Lett. **85**, 3938 (2000).

²³ R. Kleiner, T. Gaber, G. Hechtfischer, Physica C **362**, 29 (2001).

²⁴ G. Hechtfischer, R. Kleiner, A. V. Ustinov, and P. Müller, Phys. Rev. Lett. **79**, 1365 (1997).

²⁵ Yu. I. Latyshev, M. B. Gaifullin, T. Yamashita, M. Machida, and Y. Matsuda, Phys. Rev. Lett. **87**, 247007 (2001).

²⁶ L. Bulaevskii and J. R. Clem, Phys. Rev. B **44**, 10234 (1991).

²⁷ H. B. Wang, P. H. Wu, and T. Yamashita, Appl. Phys. Lett **78**, 4010 (2001).

²⁸ M.-H. Bae, H.-J. Lee, J. Kim, and K.-T. Kim, Appl. Phys. Lett. **83**, 2187 (2003).

²⁹ S. M. Kim, H. B. Wang, T. Hatano, S. Urayama, S. Kawakami, M. Nagao, Y. Takano, T. Yamashita, and K. Lee, Phys. Rev. B **72**, 140504(R) (2005).

³⁰ M. Machida, Phys. Rev. Lett. **90**, 037001 (2003).

³¹ X. Hu and M. Tachiki, Phys. Rev. Lett. **85**, 2577 (2000); Yu. I. Latyshev, V. N. Pavlenko, A. P. Orlov, and X. Hu, JETP Lett. **82**, 232 (2005).

³² A. Irie, Y. Hirai, and G. Oya, Appl. Phys. Lett. **72**, 2159 (1998).

³³ Ju H. Kim and J. Pokharel, Physica C **384**, 425 (2003).

³⁴ D. A. Ryndyk, V. I. Pozdnjakova, I. A. Shereshevskii, and N. K. Vdovicheva, Phys. Rev. B **64**, 052508 (2001).